



Al₂O₃ as a suitable substrate and a dielectric layer for *n*-layer MoS₂

Arunima K. Singh,^{1,a)} Richard G. Hennig,² Albert V. Davydov,¹ and Francesca Tavazza¹

¹Materials Science and Engineering Division, National Institute of Standards and Technology, Gaithersburg, Maryland 20899, USA

²Materials Science and Engineering, University of Florida, Gainesville, Florida 32611, USA

(Received 26 May 2015; accepted 24 July 2015; published online 5 August 2015)

Sapphire (α -Al₂O₃) is a common substrate for the growth of single- to few-layer MoS₂ films, and amorphous aluminium oxide serves as a high- κ dielectric gate oxide for MoS₂ based transistors. Using density-functional theory calculations with a van der Waals functional, we investigate the structural, energetic, and electronic properties of *n*-layer MoS₂ ($n = 1$ and 3) on the α -Al₂O₃ (0001) surface. Our results show that the sapphire stabilizes single-layer and tri-layer MoS₂, while having a negligible effect on the structure, band gap, and electron effective masses of MoS₂. This combination of a strong energetic stabilization and weak perturbation of the electronic properties shows that α -Al₂O₃ can serve as an ideal substrate for depositing ultra-thin MoS₂ layers and can also serve as a passivation or gate-oxide layer for MoS₂ based devices. © 2015 AIP Publishing LLC.

[<http://dx.doi.org/10.1063/1.4928179>]

MoS₂ has been studied for decades due to its technologically important applications in electronics,^{1–3} catalysis,^{4–6} photovoltaics,^{7–10} and lubrication.^{11–13} More recently, single- and few-layer MoS₂ have been used in field-effect transistors (FET) that exhibit high on-off ratios, exceeding 10⁸, and ultralow standby power dissipation.^{1–3} However, a major issue with MoS₂ devices is their low mobility. The measured mobilities of single layers or thin films of MoS₂ range from 0.1 to 10 cm²/V s,^{14,15} which is too low for many practical devices.

The theoretically predicted room-temperature mobility of free-standing defect-free single-layer MoS₂ is 410 cm²/V s.¹⁶ Thus, the synthesis of MoS₂ thin films with improved mobilities has been the focus of multiple studies.^{1,3,17,18} The use of high- κ gate dielectrics like Al₂O₃ or HfO₂ improves the mobility in the MoS₂ channel by 2–3 orders of magnitude. For example, MoS₂ FETs, bottom-gated with Al₂O₃, lead to high mobilities of about 100 cm²/V s,¹⁹ and of about 170 cm²/V s for top-gated structures.²⁰ Jena *et al.* have shown that this enhancement in mobility results from a suppression of Coulomb scattering of the charge carriers or a change in phonon dispersion, assuming that the band structure of MoS₂ is unchanged after placing it on Al₂O₃.¹⁸ However, very often the electronic structure of 2D materials is modified by interactions with substrates, resulting, for instance, in semiconductor to metal transition, charge doping, structural distortion, *etc.*^{21,22}

Theoretical studies of single-layer MoS₂ on Al₂O₃ have been previously reported.^{23,24} Valsaraj *et al.* studied the electronic structure of single-layer MoS₂ on oxides using the local density approximation for the exchange-correlation potential. In another work, Ji *et al.*, using density-functional theory (DFT) with the empirical DFT-D2 exchange-correlation potential, studied the energetic stabilization of MoS₂ flakes on O-terminated α -Al₂O₃ (0001) surface as a function of the rotation angle between the MoS₂ and oxide.²⁴

However, this study did not address the electronic structure of MoS₂ on the oxide substrate. Monolayer MoS₂ FETs have already been demonstrated,^{1,25} but devices based on multi-layers are promising too.³ The interface of multi-layer MoS₂ on Al₂O₃ is yet to be addressed.

In this article, using DFT with a non-local van der Waals potential, we study the interface of the α -Al₂O₃ (0001) surface and single-layer and tri-layer MoS₂ to understand the effect of high- κ dielectrics on the electronic properties of MoS₂. Using atom-projected band structures, we find that the semi-conducting nature of single- and tri-layer MoS₂ are preserved when placing it on the Al₂O₃ (0001) surface due to the weak van der Waals interaction at the interface. Furthermore, the unfolded band structures show that the band gap characters and effective masses in *n*-layer ($n = 1$ and 3) MoS₂ remain unaffected by the Al₂O₃ substrate as well. Our results confirm that the increased electron mobility in MoS₂ is caused by suppression of scattering of charge carriers, rather than a change in effective mass, or substrate-induced changes in the MoS₂ band structure.

All simulations are based on DFT using the projector-augmented wave method as implemented in the plane-wave code VASP.^{26–29} The van der Waals interactions are described by the non-local vdW-DF-optB88 exchange-correlation functional^{30–32} without considering spin-orbit coupling interactions. The van der Waals functional accurately describes the dispersion interactions in multi-layer MoS₂³³ and the physisorption of 2D materials on substrates.³⁴ The strong exciton interactions in 2D materials need to be considered to obtain optical band gaps.^{10,35,36} The band gap underestimation problem in standard DFT is overcome by hybrid functionals^{37,38} and the GW method,³⁹ but these methods have not been used in this work as there are up to 201 atoms in our simulation cells.

The adsorption energies for MoS₂ on sapphire are computed using a slab geometry with a vacuum spacing of 12 Å, which ensures that the interactions between the cells are negligible. An energy cutoff of 600 eV and *k*-point mesh density

^{a)}Electronic mail: arunima.singh@nist.gov

exceeding $20k$ -points per \AA^{-3} results in an accuracy of the binding energies of 1 meV per atom of MoS_2 . The structures are relaxed until the forces on the atoms are less than 5 meV/\AA .

Bulk MoS_2 exhibits two stable polytype layered structures, the hexagonal (2H) and the rhombohedral (3R).⁴⁰ The 2H structure has the space group $P6_3/mmc$, and its unit cell contains two S-Mo-S layers. The 3R structure with space group of $R3m$ contains three S-Mo-S layers in the unit cell. The latter is a noncentrosymmetric structure, which exhibits a valley polarization in photoluminescence emission.⁴¹ Our calculated interlayer spacing of 2H and 3R MoS_2 of 3.155 and 3.070 \AA , respectively, agrees closely with the experimental values of 2.977 and 2.983 \AA .^{42,43} We model single-layer MoS_2 as an individual S-Mo-S layer of the bulk structure (see Fig. 1(a)). Mimicking the stacking of bulk MoS_2 , tri-layer MoS_2 is modeled as the ABA and ABC stacked mono-layers of 2H and 3R MoS_2 , respectively (see Figs. 1(b) and 1(c)).

In this work, we model the sapphire substrate as a slab of Al-terminated $\alpha\text{-Al}_2\text{O}_3$ (0001) surface since large area, low-defect, and uniform flakes of MoS_2 have been experimentally grown on this surface.⁴⁴ This termination is the thermodynamically most stable termination below 1300 K and even at high oxygen partial pressure.⁴⁵ Since the surface relaxations in Al_2O_3 are large and extend up to the fifth layer from the surface, we model the substrate as a 1.2 nm thick slab with 12 Al and 6 O layers of $\alpha\text{-Al}_2\text{O}_3$ in a hexagonal unit cell, as illustrated in Fig. 1(d). The bottom 11 layers are fixed to their bulk positions, and the top 7 layers are free to relax. The inward relaxation of the topmost Al layer to the second oxygen layer is found to be 81% with respect to the bulk relaxed lattice parameters and atomic positions, in good agreement with previous DFT results.⁴⁶

First, we determine the interface structures at any rotation by identifying all symmetry-matched supercells of MoS_2 and Al_2O_3 with a surface area less than 200 \AA^2 and a lattice-mismatch of less than 5%, using the algorithm of Zur *et al.*⁴⁷ The only configuration that satisfies these constraints consists of a 2×2 supercell of Al_2O_3 that is symmetry matched with a 3×3 supercell of MoS_2 and exhibits a small lattice-mismatch of less than 0.34%. For this commensurate interface, the $[10\bar{1}0]$ directions of $\text{MoS}_2(0001)$ and $\text{Al}_2\text{O}_3(0001)$ are parallel. This is also the experimentally observed predominant epitaxial orientation of MoS_2 grown on sapphire.⁴⁴

Next, to identify the lowest energy position of the n -layer MoS_2 on the Al-terminated sapphire surface, we study three configurations: two high-symmetry configurations, top(Mo) and top(S), and a nonsymmetric configuration we call top(R). The top position refers to the site on the $\text{Al}_2\text{O}_3(0001)$ surface indicated by T in Fig. 1(d), and the Mo or S atoms of MoS_2 are placed directly above this site in the top(Mo) and top(S) configuration, respectively. For the third nonsymmetric configuration, the MoS_2 layer is shifted off the high-symmetry top(Mo) configuration by 1.5 \AA in the y -direction. We relax the n -layer $\text{MoS}_2\text{-Al}_2\text{O}_3$ for all three configurations to determine the thermodynamically most likely configurations and subsequently study their electronic structures.

The stabilization of n -layer MoS_2 by adsorption on the sapphire substrate is determined by the formation energy of the adsorbed configuration, $E_{\text{ads}}^{\text{f}} = E_{\text{vac}}^{\text{f}} - E_{\text{b}}$, where $E_{\text{vac}}^{\text{f}}$ is the formation energy of isolated n -layer MoS_2 and E_{b} is the binding energy on the sapphire substrate.^{21,22} The formation energy of isolated n -layer MoS_2 , $E_{\text{vac}}^{\text{f}}$, is defined with respect to the energy, $E_{3\text{D}}$, of bulk MoS_2 , $E_{\text{vac}}^{\text{f}} = E_{2\text{D}}/N_{2\text{D}} - E_{3\text{D}}/N_{3\text{D}}$, where $E_{2\text{D}}$ denotes the energy of isolated MoS_2 and $N_{2\text{D}}$ and $N_{3\text{D}}$ are the number of atoms in the unit cell of the single-layer and bulk structure, respectively. The interaction of n -layer MoS_2 with the substrate is given by the binding energy, $E_{\text{b}} = (E_{2\text{D}} + E_{\text{S}} - E_{2\text{D}+\text{S}})/N_{2\text{D}}$, where $E_{2\text{D}+\text{S}}$ is the energy of strained MoS_2 adsorbed on the substrate, E_{S} is the energy of the substrate slab, and $E_{2\text{D}}$ is the energy of isolated unstrained MoS_2 . The successful stabilization and synthesis of MoS_2 on Al_2O_3 are feasible when the formation energy after adsorption, $E_{\text{ads}}^{\text{f}}$, becomes negative.

Figure 2(a) shows that the adsorption of n -layer MoS_2 on sapphire results in a negative formation energy, thermodynamically stabilizing single-layer MoS_2 and tri-layer 2H- and 3R- MoS_2 . Moreover, the variation in binding energy for the three configurations of n -layer MoS_2 on Al_2O_3 is negligible. We find that the interaction strength of single-layer, tri-layer 2H- and 3R- MoS_2 with the Al_2O_3 is similar, 30 meV/\AA^2 .

The equilibrium z -separation between the top most atom of the substrate and the bottom most atom of the MoS_2 is 2.6 \AA , much larger than for single layer MoS_2 on transition metals.^{48,49} The structure of single layer as well as the tri-layer MoS_2 remain undistorted when adsorbed on the sapphire substrate. The small binding energy, negligible distortion to the MoS_2 structure, large binding distance, and weak

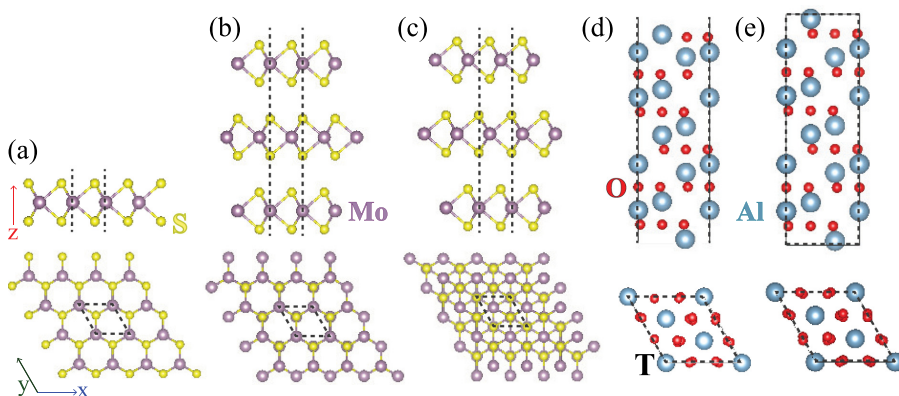


FIG. 1. Side view and top view of the crystal structures of (a) single-layer MoS_2 , (b) tri-layer 2H- MoS_2 , (c) tri-layer 3R- MoS_2 , (d) Al-terminated $\alpha\text{-Al}_2\text{O}_3$, and (e) bulk Al_2O_3 . All unit cells are shown as black dashed lines. The “top” adsorption site on Al-terminated $\alpha\text{-Al}_2\text{O}_3$ is marked as “T” in (d).

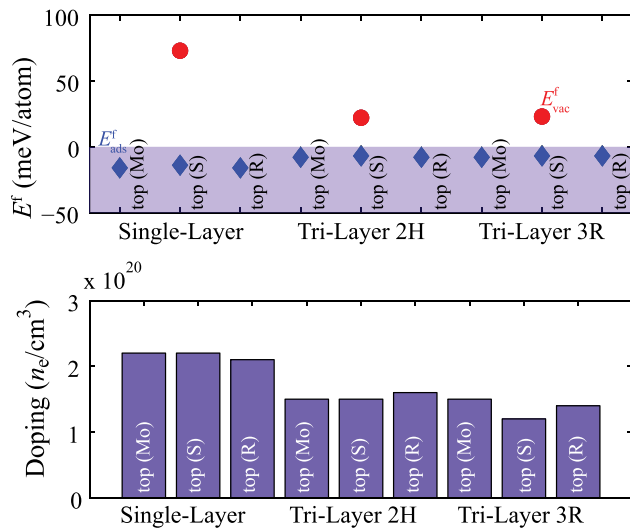


FIG. 2. (a) Formation energies of n -layer MoS₂ relative to the bulk 2H-MoS₂ for isolated n -layer MoS₂, E_{vac}^f (red circles), and for n -layer MoS₂ adsorbed on three different adsorption sites on the Al-terminated Al₂O₃ (0001) surface, E_{ads}^f (blue diamonds). The shaded region shows the regime where the few-layer MoS₂ films are stable on the oxide. (b) Electrons transferred from the sapphire substrate surface atoms to the n -layer MoS₂, a measure of the electron doping, n_e , for single-layer MoS₂, tri-layer 2H-MoS₂, and tri-layer 3R-MoS₂.

dependence of adsorption energy on the adsorption configurations indicate a weak van der Waals-type interaction between the n -layer MoS₂ and Al₂O₃.

To further confirm the bonding character between n -layer MoS₂ and the substrate, and to quantify the substrate induced doping of n -layer MoS₂, we estimate the charge transfer using the Bader formalism.⁵⁰ The Bader charges were converged to an accuracy of 0.001 by using a mesh of $160 \times 160 \times 500$. Fig. 2(b) shows the carrier density due to the electron transfer from Al₂O₃ to the MoS₂ for all the configurations. For both single-layer and tri-layer MoS₂, the charge transfer is 0.02 electrons per unit cell of MoS₂, effectively leading to carrier densities, n_e , about 10^{20} electrons/cm³. The observed charge transfer is probably a result of the extended sapphire surface states and is unlikely to be a true doping. In support, a careful inspection of the band alignments of the various surfaces and interfaces suggests the possibility of a weak substrate induced n -doping, and rules out the chance of p -doping of MoS₂.

To determine the effect of the substrate on the electronic structure of n -layer MoS₂, we calculate the atom-projected band structure of the n -layer MoS₂ isolated and adsorbed on the Al₂O₃(0001) substrate. Figures 3(a)–3(c) show the band structure of isolated, free-standing, and unstrained single-layer MoS₂, tri-layer 2H-MoS₂, and tri-layer 3R-MoS₂ projected onto the Mo atoms. Single-layer MoS₂ has a direct band gap of 1.67 eV at the K point.⁵¹ Tri-layer 2H- and 3R-MoS₂, on the other hand, exhibit an indirect bandgap from Γ to K of 1.03 and 1.04 eV, respectively. Straining n -layer MoS₂, to account for the lattice-mismatch with the Al₂O₃ surface, reduces the band gap only slightly: for single-layer MoS₂ to 1.60 eV, and for tri-layer 2H-MoS₂ and 3R-MoS₂ to 1.00 eV.⁵¹ Figure 3(d) shows the band structure of Al-terminated Al₂O₃ projected onto the Al atoms. While bulk α -Al₂O₃ is an insulator with a band gap of 6.44 eV,

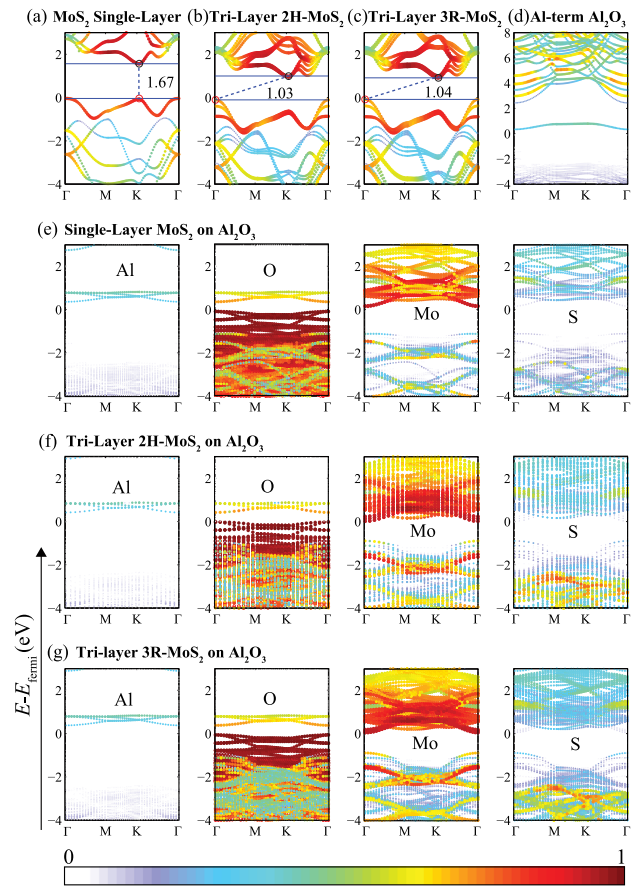


FIG. 3. Electronic band structure projected onto the Mo atoms of isolated (a) single-layer MoS₂, (b) tri-layer 2H-MoS₂, (c) tri-layer 3R-MoS₂, and onto Al atoms of (d) Al-terminated α -Al₂O₃. Band structure projected on Al-atoms, O-atoms, Mo-atoms, and S-atoms of (e) single-layer MoS₂ on Al₂O₃(0001), (f) tri-layer 2H-MoS₂ on Al₂O₃(0001), and (g) tri-layer 3R-MoS₂ on Al₂O₃(0001). The valence band maximum is set to zero. The symbol sizes and colors denote the weights of the specific atom to the bands. In (a)–(c), the blue lines indicate the valence band maxima and the conduction band minima, and the dashed lines indicate the bandgap type.

Al-terminated Al₂O₃ displays surface bonding and antibonding states in the bandgap of the bulk sapphire, see supplementary material.^{45,52}

All three configurations of n -layer MoS₂ adsorbed on Al₂O₃(0001) display nearly identical binding energies and also similar electronic band structures. Figures 3(e)–3(g) show the electronic band structure for the top(Mo) configuration, projected onto the Al, O, Mo, and S atoms. The band structures of the other configurations are shown in the supplementary material.⁵² Interestingly, the band structure of n -layer MoS₂ is only weakly affected by the interaction with the surface states of O- and Al-surface atoms in Al₂O₃. The MoS₂ remains semi-conducting without any bonding or antibonding states in its band gap.

To quantify the effect of the substrate on the electronic structure of MoS₂ on Al₂O₃, we compare the electron effective masses, m_e^*/m_0 , of n -layer MoS₂ before and after adsorption on Al₂O₃. The electron effective mass is computed as the second derivative of the band structure near the conduction band minima, at the Γ -point, of (3×3) supercells of isolated and adsorbed MoS₂. Table I shows the electron effective masses of isolated n -layer MoS₂ and n -layer MoS₂

TABLE I. Effective mass, m_e^*/m_0 , of isolated n -layer MoS₂, and n -layer MoS₂ adsorbed on Al₂O₃. m_0 is the free electron rest mass. The average scattering time of electrons, $\bar{\tau}$, is computed assuming experimentally measured mobilities.

	m_e^*/m_0	$\bar{\tau}$ (s)
Single-layer MoS ₂	0.37	2.8×10^{-15}
Tri-layer 2H-MoS ₂	0.38	2.9×10^{-15}
Tri-layer 3R-MoS ₂	0.38	2.9×10^{-15}
Single-layer MoS ₂ on Al ₂ O ₃	0.37	8.1×10^{-15}
Tri-layer 2H-MoS ₂ on Al ₂ O ₃	0.38	8.3×10^{-15}
Tri-layer 3R-MoS ₂ on Al ₂ O ₃	0.38	8.3×10^{-15}

adsorbed on Al₂O₃. The results reveal that the effective masses of n -layer MoS₂ are unaltered by the presence of the substrate.

The effective mass of the electrons is inversely proportional to the electronic mobility, $\mu = \frac{e\tau}{m_e^*}$, where τ is the average scattering time of the electrons and e is the elementary charge. The experimentally observed mobilities of MoS₂ FETs, grown on SiO₂ coated Si and passivated with Al₂O₃ film, have been reported to be 35 cm²/V s.⁵³ The mobilities decrease drastically to 12 cm²/V s when the Al₂O₃ layer is etched off. Using the calculated electron effective masses listed in Table I, the average scattering time of etched MoS₂ FETs can be estimated as 2.8×10^{-15} s and that of MoS₂ passivated with Al₂O₃ as 8.3×10^{-15} s. These results confirm that the experimentally observed increase in mobility of MoS₂ passivated by a high- κ dielectric is likely due to the reduced Coulomb scattering of charge carriers. While challenging and computationally extensive, it is worthwhile to explore the electronic structure of MoS₂ in contact with Al₂O₃ by including defects, inclusions, adsorbates, and impurities in both the materials to understand the atomic level picture of charge scattering.

Finally, we determine if the substrate affects the character of the bandgap of n -layer MoS₂ when placed on the sapphire substrate. Since, the band structure of the (3 × 3) supercells of n -layer MoS₂ adsorbed on sapphire in Figures 3(e)–3(g) is folded, it is not possible to directly identify the character of the band transitions in relation to the (1 × 1) structures. We unfold⁵⁴ the band structures using the BandUP

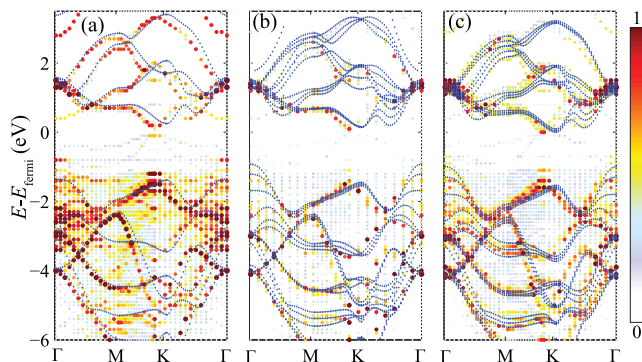


FIG. 4. The unfolded band structure of (3 × 3)MoS₂ on (2 × 2) Al₂O₃ on to the primitive (1 × 1) MoS₂ unit cell, for (a) single-layer MoS₂, (b) tri-layer 2H-MoS₂, and (c) tri-layer 3R-MoS₂. The band structure of isolated n -layer MoS₂ is superimposed, as blue diamonds. The color scale represents the number of primitive cell bands at a specific point.

code,^{55,56} and the results are plotted in Figure 4. As site projected band structures are unavailable in this implementation, some noise is present in the figure due to the states of the substrate. The band structures of the (1 × 1) primitive cell of isolated-unstrained single-layer MoS₂, tri-layer 2H- and 3R-MoS₂ are superimposed in Figures 4(a)–4(c), respectively, on the unfolded band structures as a guide to the eye. Examining the unfolded band structures with respect to the superimposed band-structures, we can clearly see that, even after adsorption on the oxide, the band transition remains direct for single-layer MoS₂, and indirect for tri-layer 2H- and 3R-MoS₂. The results reveal that indeed the electronic structure of n -layer MoS₂ is unaltered by the presence of the sapphire substrate.

In summary, we find that single-layer MoS₂ and tri-layer 2H- and 3R-MoS₂ are thermodynamically stable on the Al-terminated α -Al₂O₃(0001) surface. We demonstrate using atom-projected electronic band structures, calculations of the effective-masses, and by unfolding of the band structures that the electronic structure of MoS₂ is unaltered by the weak van der Waals interactions with the Al₂O₃ substrate. Al₂O₃ is found to be an ideal substrate for single-layer and tri-layer 2H- and 3R-MoS₂ as it thermodynamically stabilizes the n -layer MoS₂ without changing its semiconducting nature. Further, our results indicate that the experimentally observed increase in the mobility of MoS₂ when adsorbed on high- κ dielectric substrates is likely a result of decreased scattering of electrons and not due to a change in effective mass. Overall, our results will help guide future efforts to improve, engineer, and design high performance MoS₂ based nanoelectronics.

F. Tavazza and A. Davydov are funded by the Material Genome Initiative funding allocated to National Institute of Standards and Technology (NIST). A. Singh is funded by the Professional Research Experience Postdoctoral Fellowship under Award No. 70NANB11H012. The work at the University of Florida was supported by the National Science Foundation under the CAREER Award No. DMR-1056587 and under Award No. ACI-1440547, and by NIST under Award No. 00095176. This research used computational resources provided by the University of Florida Research Computing (<http://researchcomputing.ufl.edu>) and the Texas Advanced Computing Center under Contract Nos. TG-DMR050028N, TG-DMR140143, and TG-DMR150006. This work used the Extreme Science and Engineering Discovery Environment (XSEDE), which was supported by National Science Foundation Grant No. ACI-1053575. The authors thank Abhishek Motayed for illuminating discussions.

¹B. Radisavljevic, A. Radenovic, J. Brivio, V. Giacometti, and A. Kis, *Nat. Nanotechnol.* **6**, 147 (2011).

²H. Wang, L. Yu, Y.-H. Lee, Y. Shi, A. Hsu, M. L. Chin, L.-J. Li, M. Dubey, J. Kong, and T. Palacios, *Nano Lett.* **12**, 4674 (2012).

³S. Das, H.-Y. Chen, A. V. Penumatcha, and J. Appenzeller, *Nano Lett.* **13**, 100 (2013).

⁴M. Del Valle, J. CruzReyes, M. A. Borja, and S. Fuentes, *Catal. Lett.* **54**, 59 (1998).

⁵P. Faye, E. Payen, and D. Bougeard, *Mol. Model. Annu.* **5**, 63 (1999).

⁶Z. Wu, B. Fang, Z. Wang, C. Wang, Z. Liu, F. Liu, W. Wang, A. Alfantazi, D. Wang, and D. P. Wilkinson, *ACS Catal.* **3**, 2101 (2013).

⁷A. Jäger-Waldau, M. C. Lux-Steiner, and E. Bucher, *Solid State Phenom.* **37**, 479 (1994).

- ⁸M. Shanmugam, C. A. Durcan, and B. Yu, *Nanoscale* **4**, 7399 (2012).
- ⁹M. Fontana, T. Deppe, A. K. Boyd, M. Rinzan, A. Y. Liu, M. Paranjape, and P. Barbara, *Sci. Rep.* **3**, 1634 (2013).
- ¹⁰A. K. Singh, K. Mathew, H. L. Zhuang, and R. G. Hennig, *J. Phys. Chem. Lett.* **6**, 1087 (2015).
- ¹¹R. Christy, *Thin Solid Films* **73**, 299 (1980).
- ¹²M. Ripoll, R. Simi, J. Brenner, and B. Podgornik, *Tribol. Lett.* **51**, 261 (2013).
- ¹³C. Wu, S. X. Hou, H. Q. Zhang, and X. M. Jia, *Adv. Mater. Res.* **750**, 2175 (2013).
- ¹⁴K. Novoselov, D. Jiang, F. Schedin, T. Booth, V. Khotkevich, S. Morozov, and A. Geim, *P. Natl. Acad. Sci. U. S. A.* **102**, 10451 (2005).
- ¹⁵A. Ayari, E. Cobas, O. Ogundadegbe, and M. S. Fuhrer, *J. App. Phys.* **101**, 014507 (2007).
- ¹⁶K. Kaasbjerg, K. S. Thygesen, and K. W. Jacobsen, *Phys. Rev. B* **85**, 115317 (2012).
- ¹⁷M.-W. Lin, L. Liu, Q. Lan, X. Tan, K. S. Dhindsa, P. Zeng, V. M. Naik, M. M.-C. Cheng, and Z. Zhou, *J. Phys. D: App. Phys.* **45**, 345102 (2012).
- ¹⁸D. Jena and A. Konar, *Phys. Rev. Lett.* **98**, 136805 (2007).
- ¹⁹S. Kim, A. Konar, W.-S. Hwang, J. H. Lee, J. Lee, J. Yang, C. Jung, H. Kim, J.-B. Yoo, J.-Y. Choi *et al.*, *Nat. Commun.* **3**, 1011 (2012).
- ²⁰H. Li, G. Lu, Z. Yin, Q. He, H. Li, Q. Zhang, and H. Zhang, *Small* **8**, 682 (2012).
- ²¹A. K. Singh, H. L. Zhuang, and R. G. Hennig, *Phys. Rev. B* **89**, 245431 (2014).
- ²²A. K. Singh and R. G. Hennig, *App. Phys. Lett.* **105**, 051604 (2014).
- ²³A. Valsaraj, J. Chang, L. F. Register, and S. K. Banerjee, "Theoretical investigation of monolayer MoS₂ on oxide," preprint [arXiv:1412.7852](https://arxiv.org/abs/1412.7852) (2014).
- ²⁴Q. Ji, M. Kan, Y. Zhang, Y. Guo, D. Ma, J. Shi, Q. Sun, Q. Chen, Y. Zhang, and Z. Liu, *Nano Lett.* **15**, 198 (2015).
- ²⁵D. J. Late, B. Liu, H. R. Matte, V. P. Dravid, and C. Rao, *ACS Nano* **6**, 5635 (2012).
- ²⁶G. Kresse and J. Furthmüller, *Phys. Rev. B* **54**, 11169 (1996).
- ²⁷G. Kresse and J. Furthmüller, *Comput. Mater. Sci.* **6**, 15 (1996).
- ²⁸G. Kresse and J. Hafner, *Phys. Rev. B* **49**, 14251 (1994).
- ²⁹G. Kresse and J. Hafner, *Phys. Rev. B* **47**, 558 (1993).
- ³⁰J. C. V. Klimeš, D. R. Bowler, and A. Michaelides, *Phys. Rev. B* **83**, 195131 (2011).
- ³¹M. Dion, H. Rydberg, E. Schröder, D. C. Langreth, and B. I. Lundqvist, *Phys. Rev. Lett.* **92**, 246401 (2004).
- ³²G. Román-Pérez and J. M. Soler, *Phys. Rev. Lett.* **103**, 096102 (2009).
- ³³T. Björkman, A. Gulans, A. V. Krasheninnikov, and R. M. Nieminen, *Phys. Rev. Lett.* **108**, 235502 (2012).
- ³⁴J. Hwang, M. Kim, D. Campbell, H. A. Alsalman, J. Y. Kwak, S. Shivaraman, A. R. Woll, A. K. Singh, R. G. Hennig, S. Gorantla *et al.*, *ACS Nano* **7**, 385 (2013).
- ³⁵D. Y. Qiu, F. H. da Jornada, and S. G. Louie, *Phys. Rev. Lett.* **111**, 216805 (2013).
- ³⁶H. Shi, H. Pan, Y.-W. Zhang, and B. I. Yakobson, *Phys. Rev. B* **87**, 155304 (2013).
- ³⁷J. Heyd, G. E. Scuseria, and M. Ernzerhof, *J. Chem. Phys.* **118**, 8207 (2003).
- ³⁸J. Heyd, J. E. Peralta, G. E. Scuseria, and R. L. Martin, *J. Chem. Phys.* **123**, 174101 (2005).
- ³⁹G. Onida, L. Reining, and A. Rubio, *Rev. Mod. Phys.* **74**, 601 (2002).
- ⁴⁰N. Podberezskaya, S. Magarill, N. Pervukhina, and S. Borisov, *J. Struct. Chem.* **42**, 654 (2001).
- ⁴¹K. F. Mak, K. He, J. Shan, and T. F. Heinz, *Nat. Nanotechnol.* **7**, 494 (2012).
- ⁴²Y. Takeuchi and W. Nowacki, *Schweiz. Mineral. Petrogr. Mitt.* **44**, 105 (1964).
- ⁴³R. G. Dickinson and L. Pauling, *J. Am. Chem. Soc.* **45**, 1466 (1923).
- ⁴⁴D. Dumcenco, D. Ovchinnikov, K. Marinov, P. Lazi, M. Gibertini, N. Marzari, O. L. Sanchez, Y.-C. Kung, D. Krasnozhan, M.-W. Chen, S. Bertolazzi, P. Gillet, A. Fontcuberta Morral, A. Radenovic, and A. Kis, *ACS Nano* **9**, 4611 (2015).
- ⁴⁵X.-G. Wang, A. Chaka, and M. Scheffler, *Phys. Rev. Lett.* **84**, 3650 (2000).
- ⁴⁶C. Verdozzi, D. Jennison, P. Schultz, and M. Sears, *Phys. Rev. Lett.* **82**, 799 (1999).
- ⁴⁷A. Zur and T. McGill, *J. App. Phys.* **55**, 378 (1984).
- ⁴⁸W. Chen, E. J. Santos, W. Zhu, E. Kaxiras, and Z. Zhang, *Nano Lett.* **13**, 509 (2013).
- ⁴⁹J. Kang, W. Liu, D. Sarkar, D. Jena, and K. Banerjee, *Phys. Rev. X* **4**, 031005 (2014).
- ⁵⁰W. Tang, E. Sanville, and G. Henkelman, *J. Phys.: Condensed Matter* **21**, 084204 (2009).
- ⁵¹W. S. Yun, S. Han, S. C. Hong, I. G. Kim, and J. Lee, *Phys. Rev. B* **85**, 033305 (2012).
- ⁵²See supplementary material at <http://dx.doi.org/10.1063/1.4928179> for the description of the surface states of Al-terminated α -Al₂O₃ and site-projected band structures of all configurations of MoS₂ on Al-terminated α -Al₂O₃.
- ⁵³D. Sharma, M. Amani, A. Motayed, P. B. Shah, A. G. Birdwell, S. Najmaei, P. M. Ajayan, J. Lou, M. Dubey, Q. Li *et al.*, *Nanotechnology* **25**, 155702 (2014).
- ⁵⁴W. Ku, T. Berlijn, and C.-C. Lee, *Phys. Rev. Lett.* **104**, 216401 (2010).
- ⁵⁵P. V. C. Medeiros, S. Stafström, and J. Björk, *Phys. Rev. B* **89**, 041407 (2014).
- ⁵⁶P. V. C. Medeiros, S. S. Tsirkin, S. Stafström, and J. Björk, *Phys. Rev. B* **91**, 041116 (2015).